

DualFluidNet: an Attention-based Dual-pipeline Network for Accurate and Generalizable Fluid-solid Coupled Simulation

Yu Chen

Xi'an Jiaotong University

chenyu123@stu.xjtu.edu.cn

Shuai Zheng✉

shuaizheng@xjtu.edu.cn

Menglong Jin

jinml@stu.xjtu.edu.cn

Yan Chang

chang.yan@stu.xjtu.edu.cn

Nianyi Wang

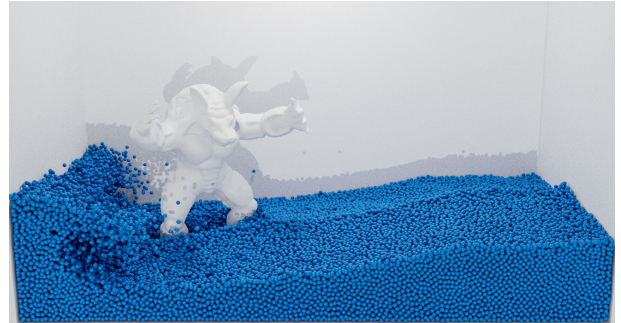
ny.wang@stu.xjtu.edu.cn

Abstract

Fluid motion can be considered as point cloud transformation when adopted by a Lagrangian description. Compared to traditional numerical analysis methods, using machine learning techniques to learn physics simulations can achieve near accuracy, while significantly increasing efficiency. In this paper, we propose an innovative approach for 3D fluid simulations utilizing an Attention-based Dual-pipeline Network, which employs a dual-pipeline architecture, seamlessly integrated with an Attention-based Feature Fusion Module. Unlike previous single-pipeline approaches, we find that a well-designed dual-pipeline approach achieves a better balance between global fluid control and physical law constraints. Furthermore, we design a Type-aware Input Module to adaptively recognize particles of different types and perform feature fusion afterward, such that fluid-solid coupling issues can be better dealt with. The experiments show that our approach significantly increases the accuracy of fluid simulation predictions and enhances generalizability to previously unseen scenarios. We demonstrate its superior performance over the state-of-the-art approaches across various metrics.



(a) Real-time rendered fluid surface



(b) Underlying simulation particles

Figure 1. Armadillo in the flowing water, with 138k particles.

1. Introduction

Comprehending physics is essential for enhancing our understanding of the environment and our interactions with it. Traditional fluid simulations have limitations in practical applications due to their high computational demands. Recent studies [3, 17, 22, 26, 29] have highlighted the potential of physics-based neural networks as a promising approach for comprehending intricate natural phenomena from data. Inspired by Smoothed Particle Hydrodynamics (SPH) methods [6, 11], which represent fluids as smoothed particles, several networks [8, 13, 19, 24, 27] have been developed for particle-based simulations. The prediction of

physical properties using neural networks is always treated as a regression problem, enabling the effective learning and approximation of physical phenomena.

While previous methods have demonstrated excellent performance in fluid simulation, we have observed that single-path networks always struggle to maintain a balance between overall particle control accuracy and adherence to physical laws. The dilemma in single-path methods turns into a trade-off issue. To deal with this problem, we propose a Dual-Pipeline Network architecture, consisting of a main pathway and a constraint-guided pathway. The main

pathway is responsible for establishing a global context and stabilizing the fluid. The constraint-guided pathway incorporates enforced constraints, learning fluid motion patterns under the physical laws. Our network seamlessly fuses the two learning ways through a meticulously designed approach, achieving a harmonious balance between these two pathways and unlocking their maximum potential. Instead of manually determining the proportion of importance for the two pathways, we employ an innovative Attention-based Feature Fusion Module, allowing the network to autonomously learn the optimal fusion between the two paths.

Although previous networks appear to perform well in handling fluid point clouds, there hasn't been an effective method for handling the mixed input of fluid and solid. Common practices involve simply concatenating the two inputs and feeding them into the network [27], or passing each through a few convolutional layers before concatenation [19]. These straightforward input concatenations are insufficient to enable the network to effectively distinguish between the features of fluid and solid particles. Nevertheless, the fluid-solid coupling is crucial for enhancing fluid simulation performance. Common feature fusion methods are frequently utilized for multimodal and multiscale fusion problems [5, 15, 31]. In the context of fluid simulation, our input comprises two entirely different features: liquid particles and solid particles. Additionally, the particle count varies in each input. We propose an innovative approach to facilitate better differentiation between fluid and solid particles in the input, enabling the network to more accurately and reliably compute their interactions during collisions. We verified that the Type-aware Input Module can be easily transferred to other network models and plays a crucial role in enhancing fluid simulation performance.

We conducted experiments on multiple 3D liquid datasets, and the results demonstrated that our network outperformed existing methods across various performance metrics, surpassing even the state-of-the-art network [19]. Furthermore, we validated the strong generalization of our network model in more challenging scenarios.

2. Related work

Comprehending physics is crucial for making sense of our surroundings and interacting with them more effectively. Smoothed Particle Hydrodynamic (SPH), representing fluids as smoothed particles, is a meshless Lagrangian method commonly employed for simulating fluid dynamics. This perspective inherently conserves fluid mass since the particle count remains constant and efficiently focuses computational resources on the fluid's location. Traditional fluid simulation methods exhibit a high level of simulation fidelity [2, 12, 25, 30, 32], but they often entail complex computations and significant computational expenses, thereby constraining their utility in situations that require real-time

predictions. In contrast, neural networks have emerged as a highly promising approach to capturing the intricacies of natural phenomena from data without incurring enormous computational costs [14, 17, 26].

A crucial consideration in employing neural networks for physics-based learning is selecting the appropriate data representation. Point clouds are widely employed in computer vision and robotics applications to represent the 3D environment [4, 20, 21, 28]. PointNet [20], which directly applies deep learning models to point cloud data, is an excellent feature extractor. However, for complex and dynamic 3D fluid simulations, a more sophisticated approach is required for accurate computation. A common approach is to utilize graph structures [1, 13, 18, 24] to create a dynamic graph connecting nearby particles, facilitating the modeling of fluid behavior. This is achieved by updating nodes and edges to simulate 'message passing' between SPH particles. Graph-based methods are strongly tied to particle discretization, but a wide range of physical phenomena, such as fluid mechanics, are governed by continuous partial differential equations (PDE) instead of discrete graph structures.

Most related to our approach is [19, 27]. [27] proposed a continuous convolution kernel (CConv) designed for establishing connections between particles and their neighbors. CConv exhibits strong learning capabilities for fluid particles and can broadly capture the dynamics of fluid motion. However, due to the absence of explicit physical constraints, its predictions may deviate from physical laws. Therefore, [19] has ingeniously designed an anti-symmetric convolution kernel building upon the continuous convolution kernel from CConv to introduce a robust constraint, allowing the network to approximate the conservation of momentum in physics during training. However, this strong constraint significantly complicates the problem for the network, leading to a reduction in its learning capacity. Single-path networks always confront this dilemma, while our dual-pipeline network excels at balancing these two distinct learning approaches, enabling our network to achieve a better equilibrium between global fluid control and adherence to physical law constraints.

3. Method

Our network follows the position-based fluids (PBF) [16] scheme. Algorithm 1 outlines the general procedure of this approach, where M_θ represents our neural network model with trainable parameters θ , and Δt represents the time interval between two consecutive time steps. Given a set of particles, denoted as p_N , where N represents the particle number, the algorithm proceeds to analyze their positions and velocities. It takes x^t and v^t as inputs, where x^t represents the positions of the particles at time step t and v^t represents their velocities. Our central learning goal is

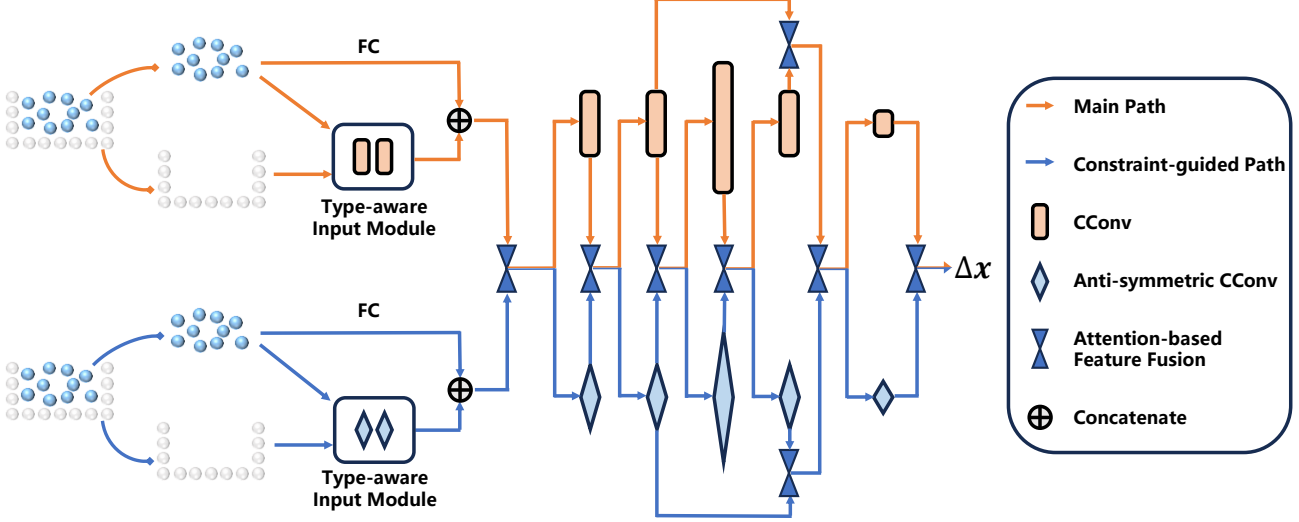


Figure 2. The architecture of our network. It consists of two pathways: the Main Path and the Constraint-Guided Path. These two pathways share a similar structure, with the Main Path utilizing CConv as its convolutional kernel (the orange rectangle), and the Constraint-Guided Path employing ASCC as its kernel (the blue diamond). At each layer, both pathways pass through a module for feature fusion before feeding the fused features into the next layer.

Algorithm 1 Simulation Process

Input : $x^t = \{x_1, x_2, \dots, x_N\}$, $v^t = \{v_1, v_2, \dots, v_N\}$
for all particles i do
 apply external forces $v_i^* \leftarrow v_i + \Delta t \frac{F_{ext}}{m}$
 update position $x_i^* \leftarrow x_i + \Delta t v_i^*$
end for
 $x^{t*} = \{x_1^*, x_2^*, \dots, x_N^*\}$
 $v^{t*} = \{v_1^*, v_2^*, \dots, v_N^*\}$
 predict position $\Delta x^{t+1} = M_\theta(x^{t*}, v^{t*})$
 update position $x^{t+1} = x^{t*} + \Delta x^{t+1}$
 update velocity $v^{t+1} = \frac{x^{t+1} - x^t}{\Delta t}$
Output : x^{t+1} , v^{t+1}

to approximate the underlying physical dynamics to predict the state of particles at the next time step $t + 1$.

3.1. Two Types of Convolution Kernels

We introduce two types of convolution kernels, denoted as CConv[27] and ASCC[19]. Given a point cloud p_N containing N points labeled as $i = 1, \dots, N$, with corresponding values f_i at positions x_i , the convolution of CConv at position $x \in p_n$ can be defined as follows:

$$\begin{aligned} CConv_g &= (f * g)(x) \\ &= \sum_{i \in \mathcal{N}(x, R)} a(x_i, x) f_i g(\Lambda(x_i - x)). \end{aligned} \quad (1)$$

Where $\mathcal{N}(x, R)$ represents the set of points located within a radius R around the position x . g is the filter function,

utilizing a mapping $\Lambda(r)$ that transforms a unit ball into a unit cube, described by [7, 27]. a is a window function applied for density normalization specific to the points x_i and x as in [10]:

$$a(x_i, x) = \begin{cases} \left(1 - \frac{\|x_i - x\|_2}{R}\right)^3 & \|x_i - x\|_2 < R \\ 0 & \text{else.} \end{cases} \quad (2)$$

ASCC can be regarded as a specialized variant of CConv, where it enforces a strong constraint through the antisymmetric kernel design, allowing it to learn fluid features while adhering to the conservation of momentum. This is achieved by halving the learnable kernel parameters along a chosen axis and determining the second half through reflection about the center of the kernel, shown in Figure 3. Notably, the mirrored values are negated. ASCC can be defined as:

$$\begin{aligned} ASCC_{g_s} &= (f * g_s)(x) \\ &= \sum_{i \in \mathcal{N}(x, R)} a(x_i, x) (f + f_i) g_s(\Lambda(x_i - x)). \end{aligned} \quad (3)$$

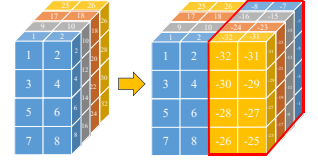


Figure 3. The anti-symmetric kernel is obtained by negating and mirroring the trainable variables by the center point.

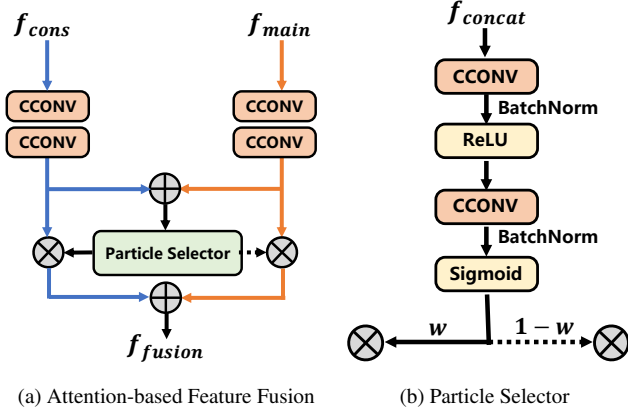


Figure 4. The schematic of the Attention-based Feature Fusion Module. Features from both pathways pass through two layers of CConv and are then concatenated. The concatenated features are subsequently input into a Particle Selector to determine the respective weights for fusion. The original features from both pathways are then combined with weighted fusion.

Where g_s represents the anti-symmetric convolution kernel and f represents the corresponding value at the position x , with the remaining symbols defined similarly to the definitions in Equation 1.

3.2. Dual-pipeline Architecture

Our network architecture is illustrated in Figure 2. Instead of manually determining the proportion of importance for the two pathways, we employ an innovative Attention-based Feature Fusion Module, allowing the network to autonomously learn the optimal connection between the two pathways. Instead of manually assigning specific weights to each pathway, we utilize an innovative Attention-based Feature Fusion Module, shown as Figure 4a, enabling the network to autonomously learn the optimal fusion between the two pathways.

More precisely, our network comprises a main pathway and a constraint-guided pathway. Both pathways share a similar structure, each comprising a Type-aware Input Module and a sequence of continuous convolutions with an effective depth of five. The main pathway, which utilizes CConv as its kernel, is responsible for establishing a global context and stabilizing the fluid. The Constraint-guided pathway employs Anti-symmetric Convolution as its kernel, which enforces a strong constraint to ensure momentum conservation while learning fluid motion patterns. Before feeding the input into the convolutional sequence, we combine the result from the input module and a fully-connected layers by addition. In the second and fourth layers of the convolution sequence, we leverage the Feature Fusion Module to implement a residual connection concept [9]. We found that these designs improve accuracy and robustness.

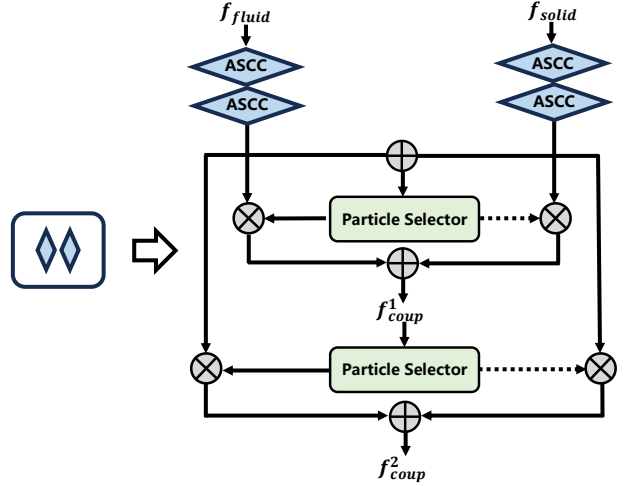


Figure 5. The schematic of the Type-aware Input Module in the Constraint-guided Path, with ASCC as the kernel. In contrast, the Main Path’s Type-aware Input Module replaces the ASCC kernel with CConv. The Particle Selector is the same as Figure 4b.

Our network seamlessly fuses these two pathways through an Attention-based Feature Fusion Module to achieve a harmonious balance between the two pathways and unlock their maximum potential. In each layer of the convolutional sequence, assuming the features from the Main Path as f_{main} and the features from the Constraint-guided Path as f_{cons} , the fusion of these two features in the Feature Fusion Module can be represented as follows:

$$f_{fusion} = S(\phi(f_{main}) \oplus \phi(f_{cons})) \otimes f_{cons} + (1 - S(\phi(f_{main}) \oplus \phi(f_{cons}))) \otimes f_{main}. \quad (4)$$

Where ϕ represents the CConv function (Equation 1). S represents the Attention-based Particle Selector and its architecture is illustrated in the 4b. With the concatenated features from the two pathways as input, the selector outputs a selection weight between 0 and 1, which is used to assess the respective significance of features from both pathways for fusion, aiming to achieve an optimal feature fusion. Unlike previous approaches, this kind of Attention-based fusion method allows our network to learn the optimal fusion between the two pathways autonomously, endowing our network with strong learning capabilities while ensuring compliance with the law of momentum conservation.

3.3. Type-aware Input Module (TaIM)

We propose an innovative approach to facilitate better differentiation between fluid and solid particles in the input, promoting a better understanding of fluid-solid coupling. Consequently, this enables the network to more accurately and reliably compute their interactions during collisions.

Figure 5 provides an example of the Type-aware Input Module architecture in the Constraint-guided Path, with ASCC as the kernel. In contrast, the Type-aware Input Module in the Main Path replaces the ASCC kernel with the CConv kernel. Unlike the Attention-based Feature Fusion Module between two pathways, the input features here represent two entirely different types, posing a greater challenge for our network to recognize their respective diverse properties. The quality of the initial fusion can significantly influence the final fusion weights. Since it is still a feature fusion problem, an intuitive approach is to employ an additional attention module for fusing these input features, which can be represented as:

$$f_{coup}^1 = S(\psi(f_{fluid}) \oplus \psi(f_{solid})) \otimes f_{fluid} + (1 - S(\psi(f_{fluid}) \oplus \psi(f_{solid}))) \otimes f_{solid}. \quad (5)$$

$$f_{coup}^2 = S(f_{coup}^1) \otimes f_{fluid} + (1 - S(f_{coup}^1)) \otimes f_{solid}. \quad (6)$$

Where ψ represents the *ASCC* function (Equation 3). f_{coup}^1 represents the output of the first attention module, while f_{coup}^2 serves as the module’s final output.

3.4. Training Procedure

Consistent with prior research [13, 24, 27], we employ a loss function that calculates the mean absolute error in position values between the predicted and ground truth weighted by the neighbor count as our loss function:

$$\mathcal{L}^{n+1} = \sum_{i=1}^N \varphi_i \|x_i^{t+1} - \hat{x}_i^{t+1}\|_2^\gamma. \quad (7)$$

Where x_i^{t+1} represents the predicted position from the Algorithm 1 at time step $t+1$, and \hat{x}_i^{t+1} represents the ground-truth position. φ_i is the weight of neighbor count to emphasize the loss for particles with fewer neighbors:

$$\varphi_i = \exp\left(-\frac{1}{c} |\mathcal{N}(x_i^{t*})|\right). \quad (8)$$

$\mathcal{N}(x_i^{t*})$ represents the neighbor count of the particle i at time step t after experiencing external force. We set $c = 40$, in accordance with the average number of neighboring particles and $\gamma = 0.5$ following [27], which makes the loss function more sensitive to small particle motions. For temporal stability considerations, we conduct training to predict particle positions for two future time steps, $t+1$ and $t+2$. This extension contributes to an overall enhancement in simulation quality. As a result, the combined loss function can be represented as follows:

$$\mathcal{L} = \mathcal{L}^{t+1} + \mathcal{L}^{t+2}. \quad (9)$$

4. Experiments

Our experiments aimed to showcase the prediction accuracy, probability distribution divergence, and inference time of our approach compared to various baseline methods. What’s more, we show the great generalization and broad applicability of our network with adequate visual analysis.

4.1. Datasets

We conducted experiments on three distinct 3D fluid datasets. Two of these datasets were derived from the Liquid3D dataset presented by [27]. The first dataset, denoted as ‘Liquid(6k),’ represents a simpler scenario with a fixed particle count of 6000. The second dataset, denoted as ‘Liquid(complex),’ encompasses a variety of complex scenarios featuring different initial shapes of fluid particles and multiple complex boxes, with particle counts ranging from thousands to tens of thousands. The Liquid3D dataset was generated using DFSPH [2], which emphasizes high-fidelity simulations and operates at a 50 Hz time resolution. It comprises 200 training scenes and 20 test scenes. The third dataset, ‘DamBreak,’ was from [13] and consists of 2000 training scenes and 300 testing scenes. These scenes simulate the behavior of a randomly positioned fluid block in a static box.

4.2. Evaluation metrics

To evaluate the prediction accuracy of each method, we calculate the average positional error by comparing the predicted positions to the ground truth. We start the assessment by using every 5th frame for initialization and compute the deviations from the ground truth between two consecutive frames, denoted as $t+1$ and $t+2$. Furthermore, we measure long-term similarity by reporting the average distance from the ground-truth particles to the closest particle in the entire sequence. This distance for frame n is computed as follows:

$$d^n = \frac{1}{N} \sum_{i=1}^N \min_{x^n \in X^n} \|\hat{x}_i^n - x^n\|_2. \quad (10)$$

Where X^n represents the set of predicted particle positions for frame n , \hat{x}_i^n corresponds to the ground-truth position for particle i , and N denotes the total number of particles. We quantify the divergence between the prediction and ground truth probability distributions by calculating the Wasserstein Distance [23] between them. The Wasserstein Distance, also known as the Earth Mover’s Distance (EMD), is a measure of the transportation cost required to transform one probability distribution into another, which can be used to measure the similarity between two distributions.

	Method	Average pos err(mm)		Average distance to closest point d^n (mm)	Wasserstein distance	Inference time(ms)
		n+1	n+2			
Liquid(6k)	DPI-Nets [13]	26.19	51.77	unstable	-	305.55
	KPConv [26]	1.65	4.54	unstable	-	57.89
	CConv [27]	0.56	1.51	29.50	0.26	16.47
	DMCF [19]	0.65	1.89	32.89	0.21	94.86
	Ours	0.43	1.16	28.32	0.17	48.01
DamBreak	DPI-Nets [13]	12.73	25.38	22.07	-	202.56
	KPConv [26]	2.49	7.05	unstable	-	47.96
	CConv [27]	0.57	1.38	20.63	0.21	12.01
	DMCF [19]	0.64	1.83	24.56	0.20	70.49
	Ours	0.42	1.02	20.90	0.18	35.57

Table 1. Quantitative Evaluation. We evaluated the networks according to the evaluation metrics described in 4.2, and also compared the inference time required per frame for each network. It’s worth noting that some methods become unstable after a few frames.

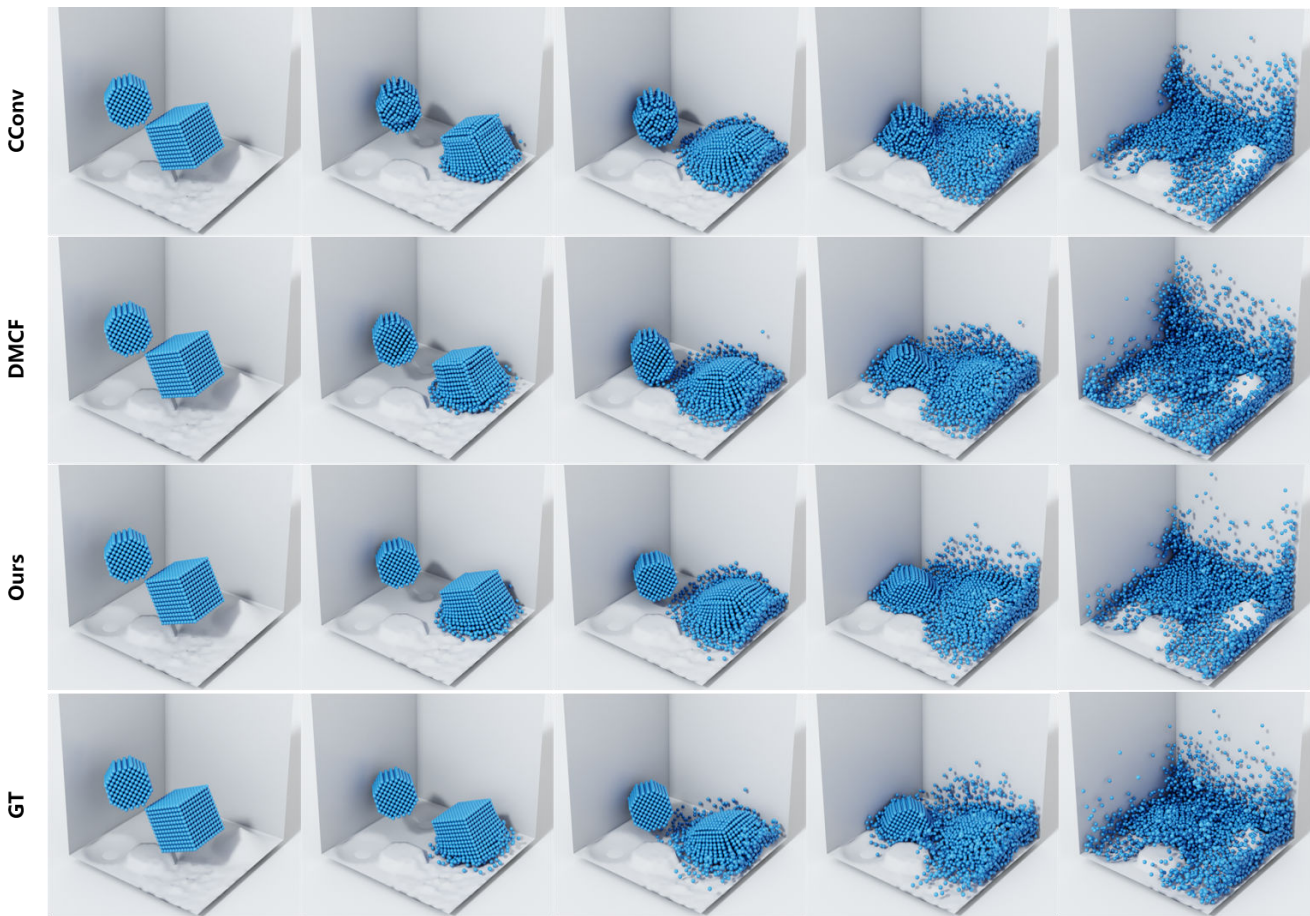


Figure 6. Qualitative Evaluation. In the results of CConv, the particles exhibit a clear overfitting to gravity. DMCF can effectively capture the physics of falling, but its ability to learn stable overall fluid dynamics is somewhat lacking, leading to occasional distortions at the edges. Our network better adheres to physical laws and reduces simulation errors, bringing it closer to the ground truth.

4.3. Comparative Experiments

Quantitative Evaluation Table 1 presents comparative experiments conducted on the Liquid(6k) and DamBreak

datasets. We assess the average error between the ground-truth particle positions and the two predicted future frames in the test set. Additionally, we calculate the average distance from the ground truth to the prediction throughout the

Method	Average pos err(mm)		Average distance to closest point d^n (mm)	Wasserstein distance
	t+1	t+2		
Main Path (no TaIM)	0.66	1.86	30.83	0.26
Main Path	0.58	1.61	30.67	0.21
Constraint-guided Path (no TaIM)	0.75	2.18	36.94	0.30
Constraint-guided Path	0.67	1.86	32.20	0.25
Ours	0.52	1.45	29.42	0.19

Table 2. Ablation Study. Our ablation experiments were conducted on the ‘Liquid (complex)’ dataset, testing the following configurations: a single Main Path without TaIM (Type-aware Input Module), a single Main Path with TaIM, a single Constraint-guided Path without TaIM, a single Constraint-guided Path with TaIM, and our final Dual-pipeline network.

Method	Average pos err(mm)		Average distance to closest point d^n (mm)	Wasserstein distance
	t+1	t+2		
CConv	0.66	1.86	30.83	0.26
CConv-TaIM	0.58	1.61	30.67	0.22
DMCF	0.73	2.08	47.89	0.21
DMCF-TaIM	0.69	2.03	46.58	0.21
Ours (no TaIM)	0.57	1.59	30.04	0.20
Ours	0.52	1.45	29.42	0.19

Table 3. The plug-and-play usability of TaIM. We incorporated TaIM as a preprocessing step before input in CConv, DMCF, and our network, and compared the performance differences with and without TaIM. We can easily integrate TaIM into networks with similar convolution kernels, resulting in a significant performance improvement. This demonstrates that the concept behind TaIM is beneficial for fluid-solid coupling.

entire sequence. The Wasserstein Distance is employed to gauge the similarity between the predicted particle distribution and the ground truth distribution.

We compare our method to DPI-Nets [13], two kinds of continuous convolution network [26, 27] and DMCF [19]. It is worth noting that DMCF exhibits an increase in mean squared error (MSE) compared to CConv [27]. This is because the anti-symmetric convolution layer introduces a strong constraint, which makes the problem considerably more challenging for the network to solve. Merely appending the ASCC at the end made it more complex to fine-tune the network to its current state. As a trade-off, the network exhibits enhanced generalization. What’s more, the Wasserstein Distance to the ground truth has also shown a decrease, indicating a distribution that more closely approximates the physically accurate ground truth. Our network outperforms in both prediction accuracy and probability distribution divergence compared to previous models. This achievement is attributed to the design of our Dual-pipeline architecture, which attains equilibrium between global fluid control and adherence to physical law constraints.

Qualitative Evaluation Figure 6 presents a visual comparison of our network with CConv and DMCF on the Liquid3D dataset. To better analyze the underlying physical principles during the dynamic simulation process, we selected five frames from the free-fall to collision with the

container’s bottom for analysis. CConv starts to deform its structure from the second frame onwards, which significantly deviates from the expected physical laws of free fall. This is attributed to CConv’s lack of emphasis on the law of momentum conservation, allowing it to overfit gravity and negate it. This reduces the problem to a local per-particle problem. In contrast, DMCF exhibits an improved adherence to the laws of physics during the free fall phase, thanks to the inclusion of ASCC. However, DMCF’s approach of simply adding ASCC as the final output layer compromises the overall stability of the fluid. This instability becomes evident from the second frame, where the edges of the cube exhibit noticeable distortion. On the other hand, our network excels in simulating the fluid by providing a stable global context while maintaining a strong grasp of physical principles throughout the simulation process, bringing it closer to the ground truth.

4.4. Ablation Study

We conduct an ablation study to assess the design choices of our network, shown in Table 2. This study employs the same evaluation metrics as the comparative experiments. We systematically analyze the contributions of each pathway independently and evaluate the enhancements provided by the Type-aware Input Module to both pathways. In addition, we also confirm the plug-and-play capability of the Type-aware Input Module. We conducted separate tests by



Figure 7. Generalization to fluid initial shapes: the Stanford Bunny fluid free-falls into a box with a circular depression at the bottom, creating splashes. See the supplementary video.

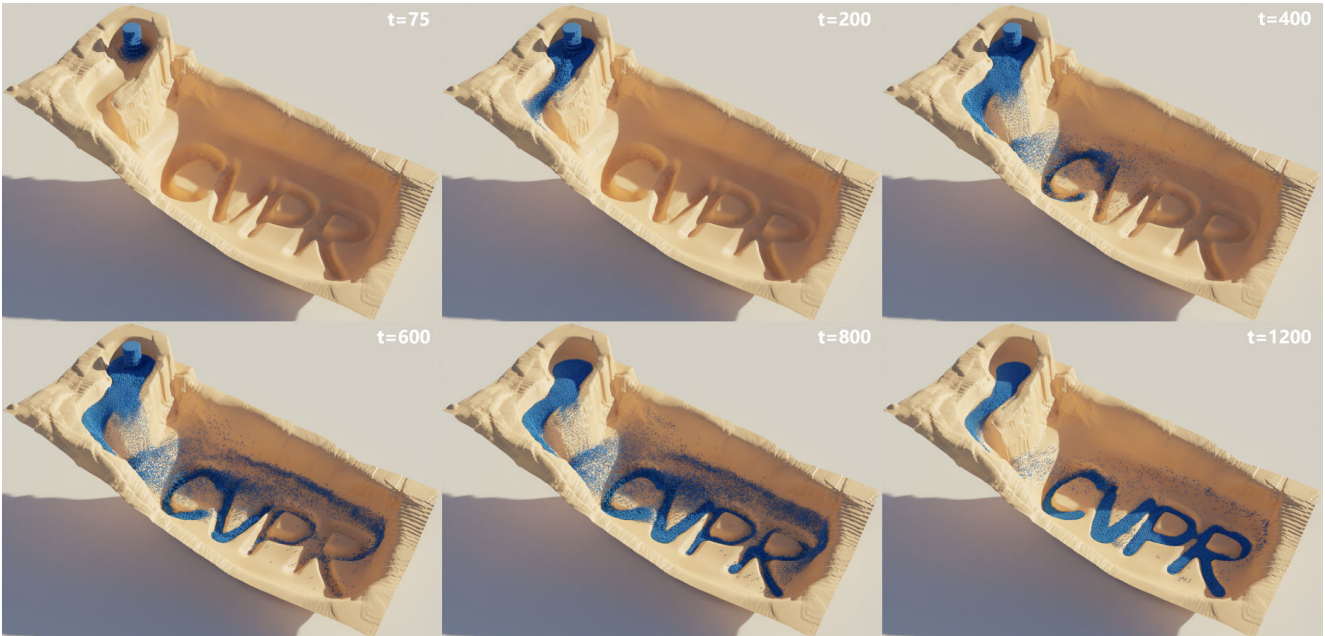


Figure 8. Generalization to complex terrains and varying fluid particle scenarios: fluid emitted from a particle emitter flows from a higher elevation in a complex valley, eventually filling the depressions in a plain. See the supplementary video.

adding this module to CConv, DMCF, and our network, as they all utilize similar convolution kernels. As illustrated in Table 3, this module proves to be instrumental in enhancing fluid simulation accuracy, indicating its pivotal role in achieving fluid-solid coupling.

4.5. Generalization

We validate the generalization capability of our network to unseen scenarios from two perspectives. Firstly, Figure 7 presents the generalization to irregular initial shapes (Stanford Bunny), which is completely unseen and full of challenges, as the initial shapes in the Liquid3D dataset are all regular. Secondly, we simulated a scenario where fluid, emitted from a particle emitter, flows from a high point in a complex valley terrain down to fill a depression in a plain, demonstrating the network’s generalization ability regarding scene geometry and the number of particles, as shown

in Figure 8. The results demonstrate the strong generalization capabilities of our method in handling complex liquid shapes and terrains. This is attributed to our Dual-pipeline architecture, which effectively learns fluid dynamics while tightly adhering to physical laws.

5. Conclusion

We have designed an Attention-based Dual-pipeline network architecture, which provides stable global fluid control and ensures adherence to physical law constraints in fluid simulation. The Dual-pipeline feature fusion architecture also holds the potential to inspire work in other domains. Additionally, we propose a Type-aware Input Module, which plays a pivotal role in facilitating the fluid-solid particle coupling. Our network represents a step forward in utilizing neural networks to simulate physically compliant fluids, enhancing the potential for real-time simulation gen-

eralization across diverse fluid scenarios, particularly in scenarios such as interactive gaming environments, and virtual reality simulations. There remains untapped potential in enabling neural networks to learn real-world physics. We will make our code publicly available to contribute to the ongoing research.

References

- [1] Peter Battaglia, Razvan Pascanu, Matthew Lai, Danilo Jimenez Rezende, et al. Interaction networks for learning about objects, relations and physics. *Advances in neural information processing systems*, 29, 2016. [2](#)
- [2] Jan Bender and Dan Koschier. Divergence-free smoothed particle hydrodynamics. In *Proceedings of the 14th ACM SIGGRAPH/Eurographics symposium on computer animation*, pages 147–155, 2015. [2](#), [5](#)
- [3] Shengze Cai, Zhiping Mao, Zhicheng Wang, Minglang Yin, and George Em Karniadakis. Physics-informed neural networks (pinns) for fluid mechanics: A review. *Acta Mechanica Sinica*, 37(12):1727–1738, 2021. [1](#)
- [4] Yu Chen and Pengcheng Shi. Rotation-invariant completion network. *arXiv preprint arXiv:2308.11979*, 2023. [2](#)
- [5] Yimian Dai, Fabian Gieseke, Stefan Oehmcke, Yiquan Wu, and Kobus Barnard. Attentional feature fusion. In *Proceedings of the IEEE/CVF winter conference on applications of computer vision*, pages 3560–3569, 2021. [2](#)
- [6] Robert A Gingold and Joseph J Monaghan. Smoothed particle hydrodynamics: theory and application to non-spherical stars. *Monthly notices of the royal astronomical society*, 181(3):375–389, 1977. [1](#)
- [7] Jens André Griepentrog, Wolfgang Höppner, Hans-Christoph Kaiser, and Joachim Rehberg. A bi-lipschitz continuous, volume preserving map from the unit ball onto a cube. *Note di Matematica*, 28(1):177–193, 2008. [3](#)
- [8] Shanyan Guan, Huayu Deng, Yunbo Wang, and Xiaokang Yang. Neurofluid: Fluid dynamics grounding with particle-driven neural radiance fields. In *International Conference on Machine Learning*, pages 7919–7929. PMLR, 2022. [1](#)
- [9] Kaiming He, Xiangyu Zhang, Shaoqing Ren, and Jian Sun. Deep residual learning for image recognition. In *Proceedings of the IEEE conference on computer vision and pattern recognition*, pages 770–778, 2016. [4](#)
- [10] Pedro Hermosilla, Tobias Ritschel, Pere-Pau Vázquez, Àlvar Vinacua, and Timo Ropinski. Monte carlo convolution for learning on non-uniformly sampled point clouds. *ACM Transactions on Graphics (TOG)*, 37(6):1–12, 2018. [3](#)
- [11] Dan Koschier, Jan Bender, Barbara Solenthaler, and Matthias Teschner. Smoothed particle hydrodynamics techniques for the physics based simulation of fluids and solids. *arXiv preprint arXiv:2009.06944*, 2020. [1](#)
- [12] Baotong Li, Honglei Liu, and Shuai Zheng. Multidisciplinary topology optimization for reduction of sloshing in aircraft fuel tanks based on sph simulation. *Structural and multidisciplinary optimization*, 58:1719–1736, 2018. [2](#)
- [13] Yunzhu Li, Jiajun Wu, Russ Tedrake, Joshua B Tenenbaum, and Antonio Torralba. Learning particle dynamics for manipulating rigid bodies, deformable objects, and fluids. *arXiv preprint arXiv:1810.01566*, 2018. [1](#), [2](#), [5](#), [6](#), [7](#)
- [14] Julia Ling, Andrew Kurzwski, and Jeremy Templeton. Reynolds averaged turbulence modelling using deep neural networks with embedded invariance. *Journal of Fluid Mechanics*, 807:155–166, 2016. [2](#)
- [15] Zecheng Liu, Jia Wei, Rui Li, and Jianlong Zhou. Sfusion: Self-attention based n-to-one multimodal fusion block. In *International Conference on Medical Image Computing and Computer-Assisted Intervention*, pages 159–169. Springer, 2023. [2](#)
- [16] Miles Macklin and Matthias Müller. Position based fluids. *ACM Transactions on Graphics (TOG)*, 32(4):1–12, 2013. [2](#)
- [17] Jeremy Morton, Antony Jameson, Mykel J Kochenderfer, and Freddie Witherden. Deep dynamical modeling and control of unsteady fluid flows. *Advances in Neural Information Processing Systems*, 31, 2018. [1](#), [2](#)
- [18] Damian Mrowca, Chengxu Zhuang, Elias Wang, Nick Haber, Li F Fei-Fei, Josh Tenenbaum, and Daniel L Yamins. Flexible neural representation for physics prediction. *Advances in neural information processing systems*, 31, 2018. [2](#)
- [19] Lukas Prantl, Benjamin Ummerhofer, Vladlen Koltun, and Nils Thuerey. Guaranteed conservation of momentum for learning particle-based fluid dynamics. *Advances in Neural Information Processing Systems*, 35:6901–6913, 2022. [1](#), [2](#), [3](#), [6](#), [7](#)
- [20] Charles R Qi, Hao Su, Kaichun Mo, and Leonidas J Guibas. Pointnet: Deep learning on point sets for 3d classification and segmentation. In *Proceedings of the IEEE conference on computer vision and pattern recognition*, pages 652–660, 2017. [2](#)
- [21] Charles Ruizhongtai Qi, Li Yi, Hao Su, and Leonidas J Guibas. Pointnet++: Deep hierarchical feature learning on point sets in a metric space. *Advances in neural information processing systems*, 30, 2017. [2](#)
- [22] Maziar Raissi, Paris Perdikaris, and George E Karniadakis. Physics-informed neural networks: A deep learning framework for solving forward and inverse problems involving nonlinear partial differential equations. *Journal of Computational physics*, 378:686–707, 2019. [1](#)
- [23] Yossi Rubner, Carlo Tomasi, and Leonidas J Guibas. The earth mover’s distance as a metric for image retrieval. *International journal of computer vision*, 40:99–121, 2000. [5](#)
- [24] Alvaro Sanchez-Gonzalez, Jonathan Godwin, Tobias Pfaff, Rex Ying, Jure Leskovec, and Peter Battaglia. Learning to simulate complex physics with graph networks. In *International conference on machine learning*, pages 8459–8468. PMLR, 2020. [1](#), [2](#), [5](#)
- [25] Barbara Solenthaler and Renato Pajarola. Predictive-corrective incompressible sph. In *ACM SIGGRAPH 2009 papers*, pages 1–6. 2009. [2](#)
- [26] Jonathan Tompson, Kristofer Schlachter, Pablo Sprechmann, and Ken Perlin. Accelerating eulerian fluid simulation with convolutional networks. In *International Conference on Machine Learning*, pages 3424–3433. PMLR, 2017. [1](#), [2](#), [6](#), [7](#)

- [27] Benjamin Ummenhofer, Lukas Prantl, Nils Thuerey, and Vladlen Koltun. Lagrangian fluid simulation with continuous convolutions. In *International Conference on Learning Representations*, 2019. [1](#), [2](#), [3](#), [5](#), [6](#), [7](#)
- [28] Yue Wang, Yongbin Sun, Ziwei Liu, Sanjay E Sarma, Michael M Bronstein, and Justin M Solomon. Dynamic graph cnn for learning on point clouds. *ACM Transactions on Graphics (tog)*, 38(5):1–12, 2019. [2](#)
- [29] Michael Woodward, Yifeng Tian, Criston Hyett, Chris Fryer, Mikhail Stepanov, Daniel Livescu, and Michael Chertkov. Physics-informed machine learning with smoothed particle hydrodynamics: Hierarchy of reduced lagrangian models of turbulence. *Physical Review Fluids*, 8(5):054602, 2023. [1](#)
- [30] Ting Ye, Dingyi Pan, Can Huang, and Moubin Liu. Smoothed particle hydrodynamics (sph) for complex fluid flows: Recent developments in methodology and applications. *Physics of Fluids*, 31(1), 2019. [2](#)
- [31] Zixiang Zhao, Haowen Bai, Jianshe Zhang, Yulun Zhang, Shuang Xu, Zudi Lin, Radu Timofte, and Luc Van Gool. Cddfuse: Correlation-driven dual-branch feature decomposition for multi-modality image fusion. In *Proceedings of the IEEE/CVF Conference on Computer Vision and Pattern Recognition*, pages 5906–5916, 2023. [2](#)
- [32] Shuai Zheng, Fan Gao, Ziyu Zhang, Honglei Liu, and Baotong Li. Topology optimization on fuel tank rib structures for fuel sloshing suppression based on hybrid fluid–solid sph simulation. *Thin-Walled Structures*, 165:107938, 2021. [2](#)